DESIGN AND IMPLEMENTATION OF LASER POWDER BED FUSION ADDITIVE MANUFACTURING TESTBED CONTROL SOFTWARE[i]

Ho Yeung[1*], Keely Hutchinson[1,2], Dong Lin[2]

[1]National Institute of Standards and Technology, Gaithersburg, MD 20899
[2]Kansas State University, Manhattan, KS 66506

Abstract

The National Institute of Standards and Technology developed a facility titled the Additive Manufacturing Metrology Testbed to advance the research in laser powder bed fusion (LPBF) processes. The testbed adopted an open control architecture which allows full access to all key process parameters. Although LPBF control is a very important topic, very little literature can be found on how this is implemented. This paper reviews the testbed control software design and implementation. Scan path planning, galvo motion control, and laser power control are detailed with select highlights. Comparison with commercial machine control software is made, and recent experiments utilizing the advanced features of the testbed control software are also discussed.

Introduction

Additive manufacturing (AM) technology has evolved from its early use in preproduction prototyping to being used regularly to fabricate parts used in many industries, including aerospace, medical, and automotive. It is very useful for creating parts that are too difficult or even impossible to manufacture traditionally. One type of AM process is laser powder bed fusion (LPBF) [1], in which a laser is used to selectively fuse a thin layer of metal powder into cross-sections of the intended three-dimensional (3D) structure. This process is repeated after each successive layer of metal powder is spread on top of the completed layer, until the 3D structure is completed. The inherent resulting part quality is determined by many process parameters, such as powder layer thickness, hatch distance, laser spot size, scan path, power, and velocity [2].

A major quality issue in additively manufactured parts is pores, that can deteriorate a part's performance and can cause part failure. Pore formation has been attributed to various phenomena related to the power-speed (P-V) settings, such as keyhole collapse at high laser energy densities [3,4], or insufficient re-melting of adjacent scan vectors [5,6]. The residual stress caused by the very localized rapid heating and cooling cycles in AM is another important issue; it generates distortion and dramatically deteriorates functionality of the additively manufactured parts [7,8]. The thermal history of the AM metal part is also known to affect its microstructure [9,10]. Although AM and specifically LPBF have come a long way and have made significant strides in

---

recent years, there are still many opportunities to improve the part quality by optimizing the process parameters and scan strategies.

The National Institute of Standards and Technology (NIST) developed the Additive Manufacturing Metrology Testbed (AMMT) to advance monitoring, controls, and metrology research in LPBF [11]. The AMMT control implementation follows the open platform AM process control framework shown in Figure 1. The framework consists of two major parts: the AM software part and the hardware part. The AM software part generates time-stepped digital commands from a computer aided design (CAD) model through slicing, path/power planning, and interpolation steps, and checks the commands created by simulation. Time-stepped digital commands are commonly used in computer numerical control (CNC) where the device status is updated at a regular time interval. The hardware part executes the digital commands through the synchronized actions of the laser system, powder bed, build chamber, and monitoring devices. Feedback/feedforward control loops can be implemented based on the signals from the monitoring devices.
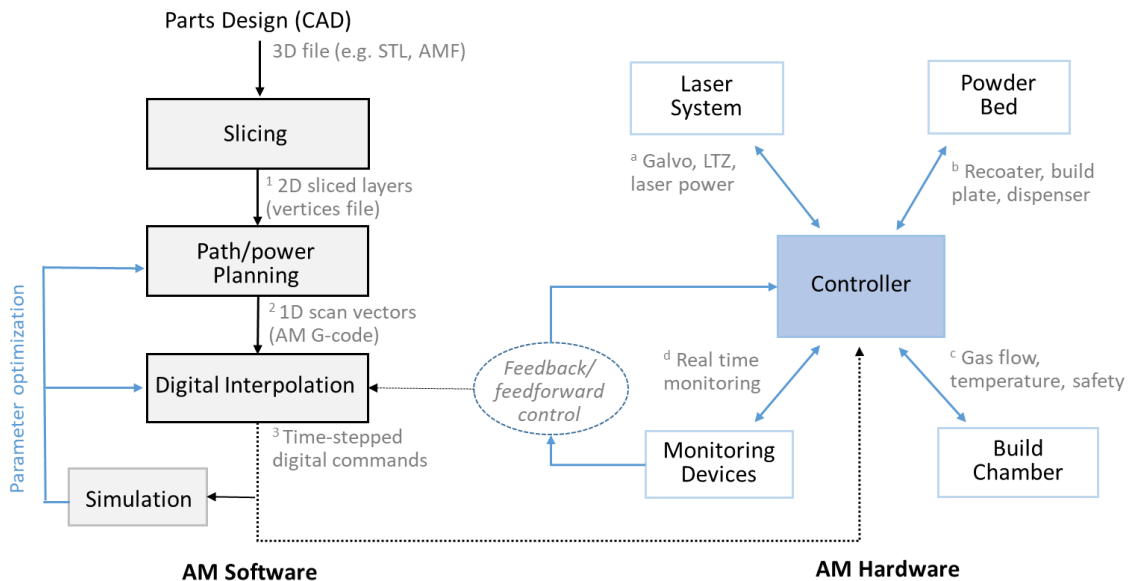

Figure 1: Open platform AM process control framework. The framework consists of four AM software modules and four hardware modules. The interfaces of each software module and functionalities of each hardware module are indicated.

In this paper, we focus on the design and implementation of the four AM software modules, namely, slicing, path/power planning, digital interpolation, and simulation (Figure 1). Collectively, we name these four modules as 'SAM', or Simple Additive Manufacturing software. SAM provides a reference architecture for an open platform AM control software, which allows researchers to create and test a wide variety of scan strategies, which would otherwise be limited if a commercial machine was used to perform this research. The rest of the paper is divided into three sections: (1) Design and implementation of the SAM; (2) Investigation of scan control on commercial systems; (3) Case studies on the advanced scan strategies implemented with SAM.

Simple Additive Manufacturing software (SAM)

SAM is an open platform AM preparation software developed for use with the NIST AMMT. SAM slices a 3D model into 2D layers, fills the layers with scan paths, creates G-code [12] to describe the scan path, and interprets the G-code path into time-stepped digital commands to drive the testbed. SAM's interface follows closely the framework from Figure 1. The SAM interface compared side-by-side with this framework is shown below in Figure 2.
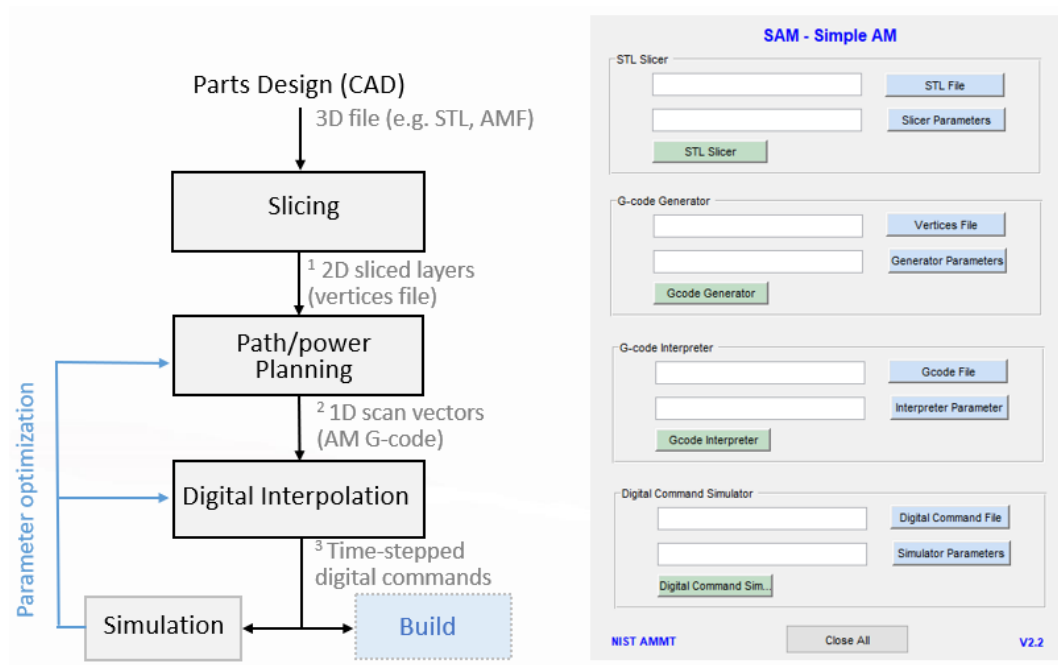

Figure 2: SAM interface compared side-by-side with the open platform process control framework.

The SAM interface is 'simple.' It consists of four clear modules. Each module takes two input files: a parameter file and a data file. The parameter file contains parameters and options required to process the data file. The parameter file is in a simple comma separated variable (CSV) format, all parameters and options are user definable. The STL slicer module takes a STereoLithography (STL) file as the input data file and generates a vertices file which contains vertices of all sliced layers. The G-code generator module takes a vertices file from the previous step as the input data file and generates a G-code file which describes the scan path and power. The G-code interpreter module takes a G-code file from the previous step as an input data file and generates a digital command file which contains the laser position, power, and diameter command at 10 µs time-steps. This time-stepped digital command file can be sent either directly to the AM controller to build the part, or to the Simulator module to check the file.

Each SAM module can also run independently and take a data input file created by a third-party software as long as it follows the same syntax. For example, the SAM G-code interpreter can be used to interpret G-code created by a material extrusion slicer. Obviously, the laser control is missing in the G-code created by a material extrusion slicer but can be easily added, as a G-code file can be created/edited by any text editor. Therefore, the well-defined data file formats, the readiness of third-party software interface, and the easy accessibility of all the control parameters,

make SAM a truly open platform AM software. Next, we will go through each SAM module in detail.

STL Slicer

The first module of the SAM is the STL slicer. STL defines a series of linked triangles to reproduce the surface geometry of the 3D model. STL slicer finds intersect points of the triangles to the layers of constant height parallel to the build plane, and connects the adjacent points on the same layers to create the boundaries for the cross-sections. Figure 3 shows a visual representation of the STL slicing, where Figure 3a-c show a CAD model of a tensile bar, its STL representation, and the parallel slicing planes, respectively. The cross-section boundary created by the intersection of one of the slicing planes with the STL triangles is shown in Figure 3d. Note the boundary consists of only straight-line segments, this is the limitation of the STL representation. If two adjacent line segments are collinear, they can join together to reduce the redundant points as shown in Figure 3e. In order to restore the cylindrical surface, an arc-fitting algorithm is applied as shown in Figure 3f. SAM is able to perform arc motion such as G02 and G03 commands in G-code [12,13]. This greatly improves dimensional accuracy for surfaces with curvature.
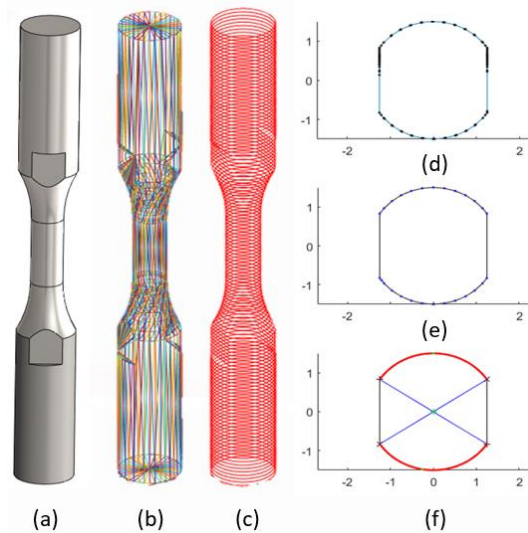

Figure 3: STL slicing. (a) CAD model of a tensile test bar. (b) STL /triangle representation of the CAD model surface. (c) Parallel slicing planes. (d) The boundary of a cross-section outlined by the intersect points (black) resulted from a slicing plane and STL. (e) Collinear segments joined. (f) Arc-fitting to restore the surface with curvature.

Parameters such as the layer heights, starting and ending layers, and arc-fitting tolerance can be customized in the parameter file for this module. The output of this module is a binary file containing vertices of all sliced layers, with a mark-up to specify whether the two adjacent points are connected by a straight line or an arc. If it is an arc, the center and radius of the arc are also specified. This vertices file provides all necessary geometric information for the next step, the G-code generation.

G-Code Generator

The next module of SAM (Figure 2) is the G-code generator, which generates AM G-code that describes the scan path and power used for each layer. The AM G-code is a slightly modified version of the RS-274 standard [14]. It adds keywords 'L' for laser power, and 'D' for laser diameter control. An example is shown in Figure 4, where the laser is commanded to go linearly (G01) to coordinate (X=5, Y=0) with speed (F) = 1000 mm/s, laser power (L) = 200 W, and laser diameter (D) = 2 times of the default setting. The L and D keywords allow the nominal laser power and diameter to be set for each scan line, which allows more flexibility in scan strategy implementation. In addition to linear motion (G01), arc motions (G02 and G03) and dwell (G04) are also implemented following the RS-274 standard. A new capability is also developed to realize spiral paths in Figure 5a.

A (0,0)　　　　　B(5,0)　　　　G01 X5 Y0 F1000 L200 D2

Figure 4: An example line of AM G-code defining a move of the laser.

There are many options for the path and power planning in SAM; they are summarized in Figure 5. Four sample hatching patterns are shown in Figure 5a. In a raster pattern, evenly spaced parallel lines are used to fill the region being built. In a concentric pattern, the region is filled by a series of concentric contours. The concentric spiral pattern is similar, but it spirals in with a continuous scan path. The shift spiral pattern is a moving circular path, which leaves a fully melted stripe behind. Different hatching patterns can be applied between layers. There are more detailed parameters that can be edited to more fully describe how these paths are carried out. Certain patterns may not fit completely to the region being built, so a 'power mask' is implemented to shut off the laser power instead of disrupting the scan motion when it goes beyond the part boundary. Therefore, these hatch patterns can be applied to any shape.

Two examples of hatching power modes are shown in Figure 5b. On the left is the interleaved power mode, which scans every other line on the first pass, and the remaining lines on the second pass. On the right is alternative power mode, in which the laser power is alternated between two power levels on sequential scan lines. These modes can be controlled in detail using the parameters file. There are also options for the island strategy that allow the region to be divided into rectangles of any size, and scanned in different sequences with different inter-island rotation angles, as shown in Figure 5c. The same layer can be scanned multiple times, with different power levels, laser diameters, and hatch space settings, as shown in Figure 5d. There are also options in SAM to set layer-wise scan strategies, such as different nominal power and speed, and interlayer rotation angle for different layers. Many of these options can also be combined to create highly customized scan strategies for different research needs. The output of this module is an AM G-code file. This output can also be further customized by the user before its interpretation.
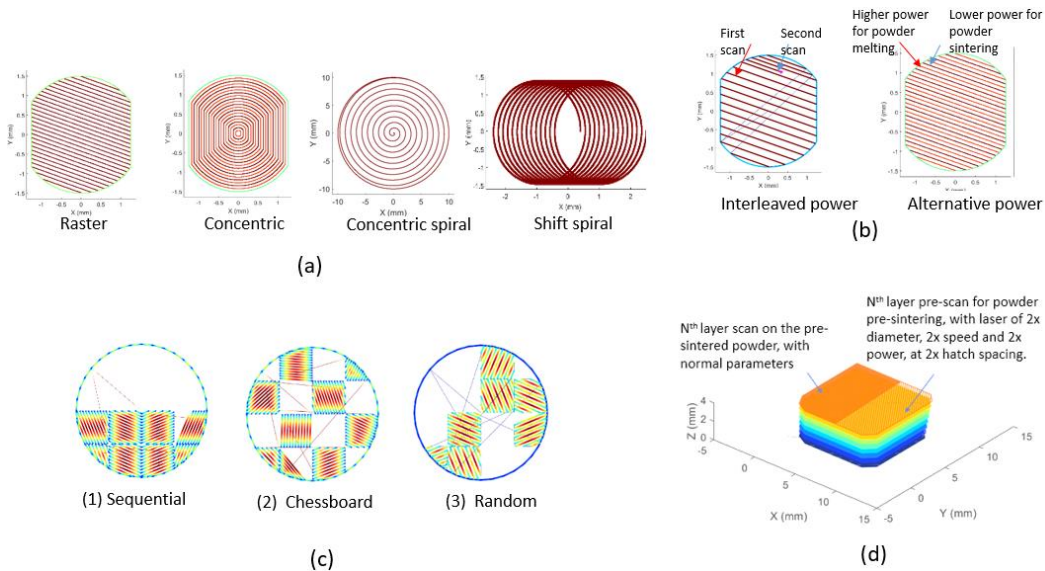
Figure 5. Examples of path/power planning modes available for use in SAM. (a) Hatching patterns. (b) Hatching powers. (c) Island sequence. (d) dual scans.

G-Code Interpreter

AM G-code contains information of destination, nominal speed, nominal power, and nominal spot size. It needs to be converted into a time-stepped digital command for the AM controller to execute. This conversion is carried out in the G-code interpreter module. The time-stepped digital command file in SAM is defined as an n x m numerical array as shown in Figure 6a, where n is the number of time steps in 10 µs increments, and m is the number of control parameters. The command format is based on the xy2-100 protocol [18] for galvo position (X, Y), but extended to laser power (L), laser diameter (D), and trigger for monitoring devices (T). One line of the commands is executed by the AM controller at every 10 µs (Figure 6b), which sends the update to each controlled device (Figure 6c).

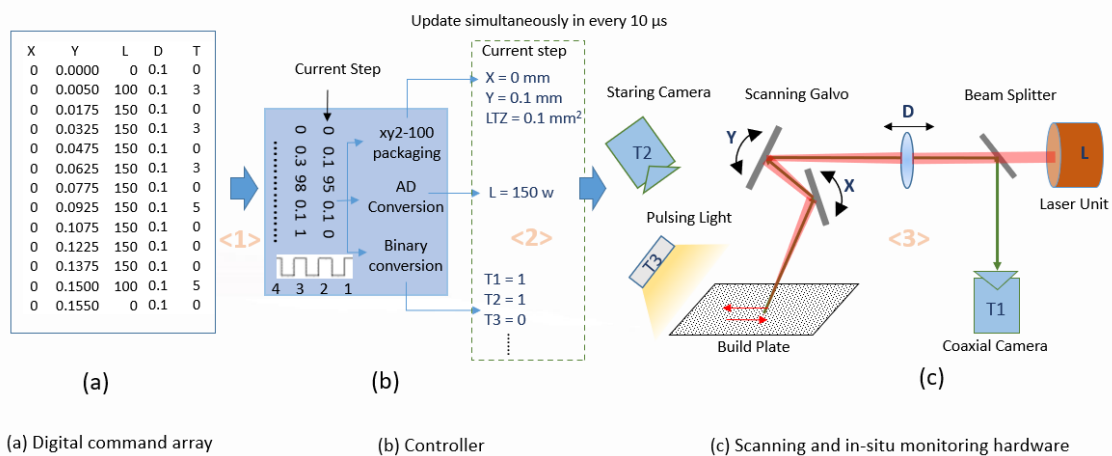
Figure 6. Time-stepped digital command and its execution. (a) Command format. Each column is a control parameter. (b) Command execution. Every 10 µs a line is sent for execution. (c) Devices controlled.

To interpret G-code into time-stepped digital commands, three interpretation modes are defined. (1) Velocity mode for motion control. (2) Path mode to handle the beginning and end of a scan. (3) Power mode to synchronize the laser power to motion. Figure 7 shows the three velocity modes implemented in SAM. Step velocity (Figure 7a) is the easiest to program but it requires an infinite acceleration, which no physical system can deliver. Trapezoidal velocity (Figure 7b) allows time for the velocity to pick up, but it assumes the required acceleration can be reached instantaneously. For the galvo (a DC motor), the torque/acceleration is proportional to the current flow through the armature. The DC motor is a second-order system, it does not allow a jump in current. Therefore, the time derivative of the acceleration, which is known as jerk, cannot be infinite. An infinite acceleration or jerk will cause deviation of the actual velocity from the commanded velocity and hence cause the following error. Jerk-limited velocity (Figure 7c) gives the best spatial and temporal accuracy [15], but it is also the most computational intensive to program.
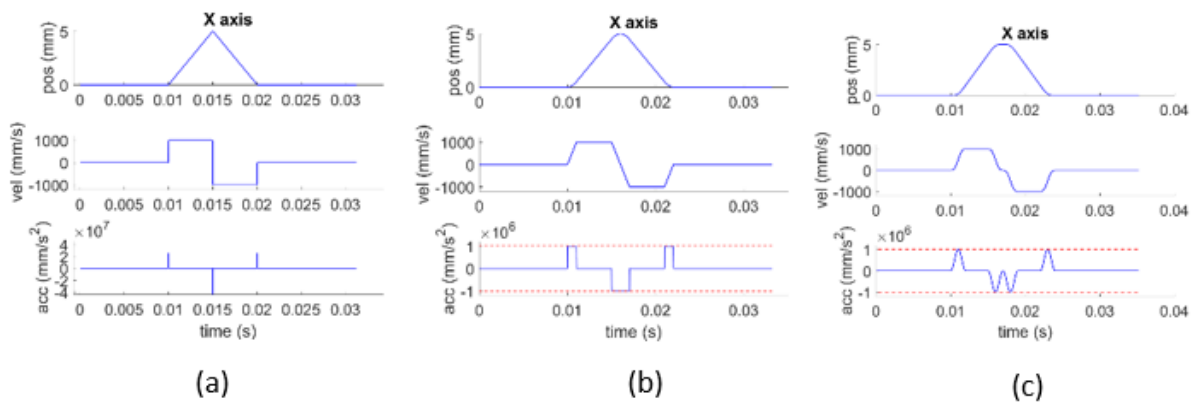

Figure 7: Position, velocity, and acceleration graphs for (a) step velocity, (b) trapezoidal velocity, and (c) jerk-limited velocity profile. The jerk-limited velocity here is implemented with a sinusoidal acceleration.

Figure 8 shows the three path modes defined in SAM. The exact stop mode (Figure 8a) stops motion exactly at the end of each scan with maximum allowable deceleration, and the laser power is switched off when the motion is stopped. If there is a subsequent scan, the motion will start again immediately with maximum allowable acceleration until it reaches the nominal speed (set in AM G-code by keyword F), or until it needs to decelerate again. The constant build speed mode (Figure 8b) keeps the programmed speed at the end of the current scan, and adds a colinear deceleration path to stop the galvo. It also adds a colinear acceleration path to the start point of the next scan, to speed up the galvo to the programmed speed. The laser power is turned off during these deceleration/acceleration paths. It is named constant build speed mode since whenever the laser power is on, the scan speed is constant. The continuous mode (Figure 8c) matches the ending velocity of the scan with the beginning velocity of the subsequent scan. To do so, an arc is used to join two adjacent scans (hatch lines). The laser power is kept on, hence the meltpool is also continuous [16].
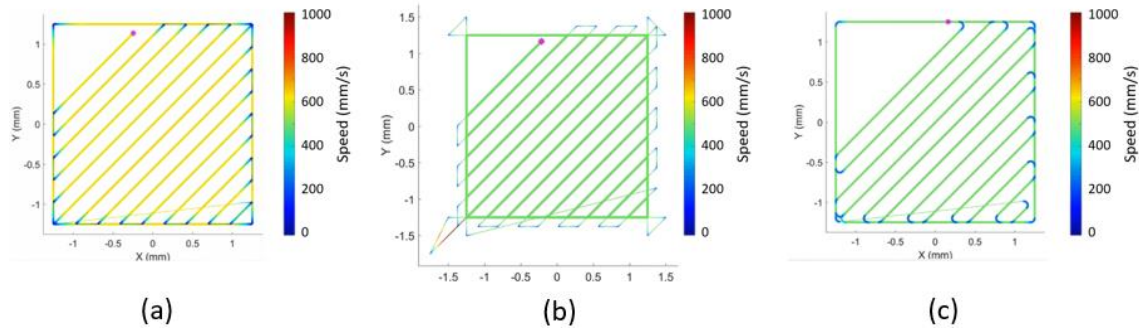
Figure 8: Speed plot for the three path modes. The thicker lines indicate where the power is on, the pseudo color indicates the speed. (a) Exact stop. (b) Constant build speed. (c) Continuous.

Three power modes are also defined in SAM: constant power, constant power density, and thermal adjusted power. Constant power mode keeps the power constant at the nominal level (set in AM G-code by keyword L) for the whole scan line. Constant power density mode keeps the power/speed ratio (power density) constant within a scan line. The thermal adjusted power mode compensates for the local variation of thermal property by changing the laser power. It also provides a means for model-based feedforward control of the laser power. Users can also develop their models as plug-ins.

The AM G-code interpretation and time-stepped digital command file enables continuous laser power control, complicated scan path implementation, and model-based scan strategy optimization. The use of the time-stepped digital command also makes the AM process fully transparent. The digital command file alone contains all the information required to build a part, and hence supports the cross-platform operation. It will be shown later that the digital commands intercepted on a commercial system can also be executed on AMMT.

Simulator

AM is a very expensive process. Parts usually take hours if not days to build. It is crucial to examine the build files to make sure there are no design errors. The simulator reads the time-stepped digital commands, simulates the scan, and displays the result graphically for the user to examine. Figure 5, Figure 7, and Figure 8 are prepared with the Simulator. More sophisticated simulations, such as the galvo dynamic response and meltpool behavior, are under development.

Commercial Systems

For an LPBF AM system, the heating laser is guided to the build platform by a pair of mirrors driven by galvo motors. Figure 9 shows a simplified schematic of the scan control. The AM scan paths, which are a series of x-y position pairs, are created by AM preparation software. These positions are then interpolated into time-stepped digital commands and transmitted through digital communication lines following the xy2-100 protocol. The digital/analog (D/A) receiver then converts the digital commands received to analog voltages to move the mirrors, and thereby moving the laser beam through the galvo driver board. On most commercial machines, however, the system described in Figure 9 acts as a black box. The user has limited control over how the

scan path is created and interpolated. To understand the scan strategy and control on these commercial systems, one approach is to tap into the xy2-100 digital communication line (Figure 9) and intercept the digital command. From these digital commands, the scan strategy can be reconstructed.
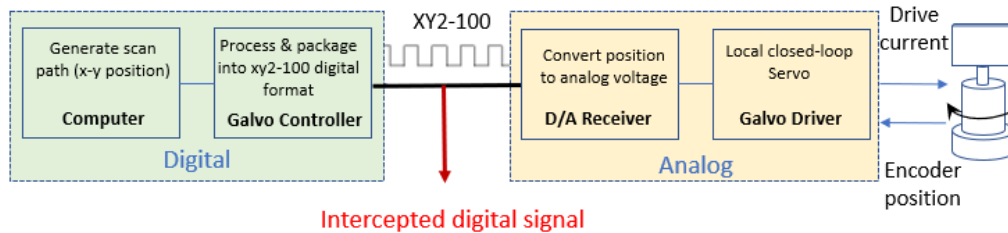

Figure 9: The schematics show AM scan control. The red arrow shows where the digital command signal can be intercepted.

Figure 10 shows the scan strategy read from a commercial LPBF AM machine, where single tracks are scanned, and the digital commands are intercepted. The programmed scan path is shown in Figure 10a, and the scan path constructed from the captured digital signal is shown in Figure 10b. The x-displacement, x-y speed, and acceleration are plotted in Figure 10c. The nominal scan speed is 200 mm/s, but it can be seen there are jumps with a speed of approximately 5000 mm/s and acceleration of 5×10^8 mm/s^2. The acceleration requires increasing the speed from 200 mm/s to 5000 mm/s in one 10 µs time step; therefore a step velocity profile was applied for the motion control. No galvo system can deliver this acceleration; therefore the following error must occur at the jump. Nevertheless, it should be pointed out that the following error does not necessarily cause a build issue, as long as the laser power is not on.
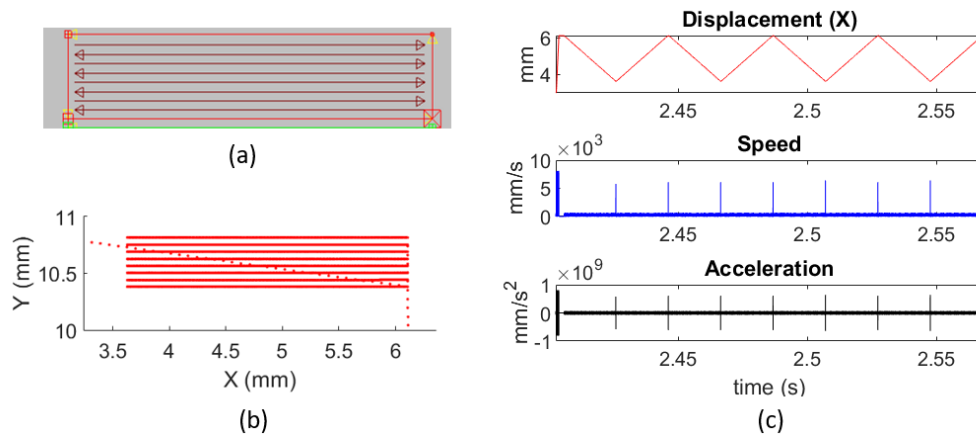

Figure 10: Scan strategy read from a commercial LPBF AM machine for single tracks. (a) Programmed scan path. (b) Scan path constructed from digital command intercepted. (c) X-displacement, x-y speed, and x-y acceleration.

Figure 11 shows the scan strategy read from a commercial LPBF AM machine of a different model, where a square pad was scanned (Figure 11a). The initial infill and the contour regions are shown in Figures 3b and 3c, respectively, alongside the speed and acceleration plots. The laser power is recorded simultaneously, and the path taken with the laser on is plotted in red. The infill is programmed at 750 mm/s and the contour at 400 mm/s. Again, a step velocity profile

is applied for the motion control. For the infill, jumps are observed at the beginning/end of every hatch line (Figure 3b), but they do not happen immediately before/after the laser power is turned on/off. An extension (overshoot) of the path is inserted at the beginning/end of the scan to allow the system to recover from the following error caused by the jump. Therefore, during the build (when the laser power is on) the scan speed remains constant. This strategy is known as skywrite on some commercial machines. This is very similar to the constant build path mode of SAM, except this extension path is at a constant speed, not an accelerate/decelerate path that SAM uses.

However, the contour is scanned at a constant speed without overshoot. It is uncertain if the sharp turn at the corner can be followed, but the effect on part geometry is likely minimal since the area will be melted again by the infills. Step velocity simplifies the interpretation, but a significant following error is unavoidable. The potential build issues can be avoided by carefully designed/calibrated scan strategies such as the skywrite here, but this also imposes restrictions on the scan strategy design.
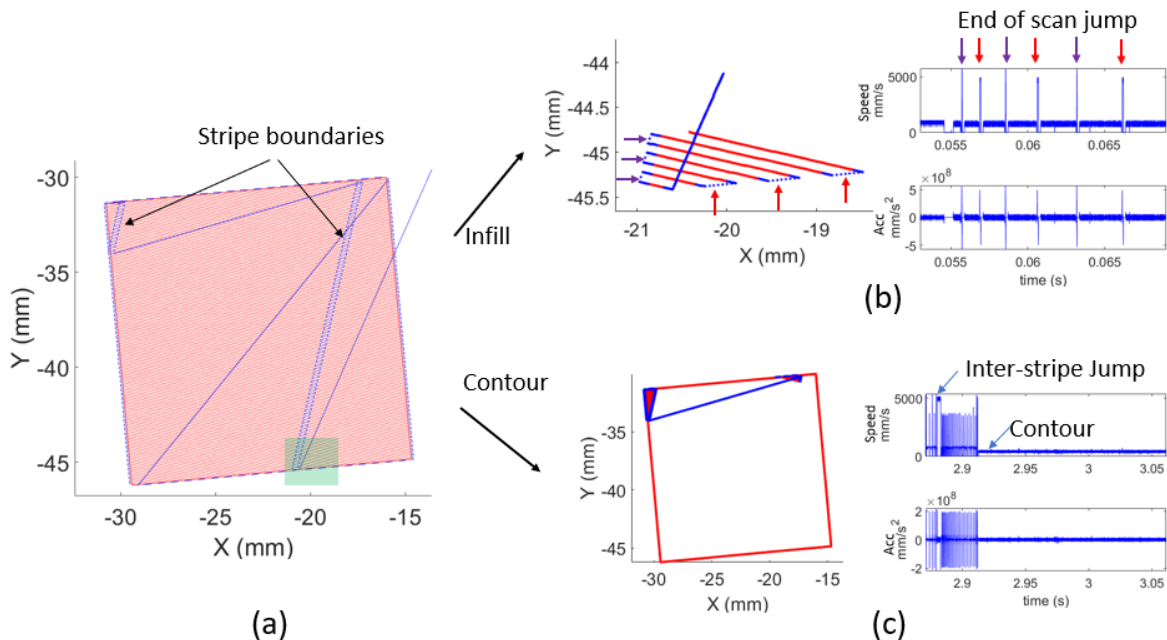

Figure 11: Scan strategy read from a commercial LPBF machine for a square pad. (a) Scan path constructed from digital command intercepted. The path with laser power-on is plotted in red. (b) Enlarged infill path for the shaded region in (a). The end-of-scan jumps are marked by arrows on the x-y speed plot on the left. (c) The contour, no overshoot is observed.

The galvo position read by tapping into the xy2-100 digital communication line is the commanded position. The actual galvo position can be measured by reading the galvo position encoder feedback (Figure 9). However, the galvo encoder signal is not easily accessible on commercial machines. Since AMMT has already built in the capability to capture the galvo encoder position, a commercial AM controller can be used to drive AMMT. The behavior of this commercial AM controller is studied by comparing the commanded and measured galvo positions (measured by the galvo position encoder).

Figure 12a shows how an 8 mm square is scanned on AMMT driven by a commercial AM controller. The controller software provides a graphic user interface (GUI) to define the scan path, speed, and power. Both the commanded and measured positions were captured and plotted in Figure 12a in blue and orange, respectively. The position, speed, and acceleration plots in the figure show that a step velocity profile is used for the command, and the sharp corner of the commanded position could not be followed. This is shown in the speed plot in Figure 12a. It is surprising to see that during the turn, the scan is commanded to idle for a short moment after the current line stops and before the next line starts, while the power is still on. It is marked by 'X stop' and 'Y start' in the position plot in Figure 12a. This idle is believed to be inserted by the controller to ensure that the current line is completed before the next line starts, to maintain a sharp corner (geometric accuracy), although this results in an overheated region at the corner. Figure 12b shows the same square scanned with SAM software and AMMT controller. The ramp velocity profile is used for the motion control. The position and velocity profiles are better followed. In this case, the improved temporal accuracy allows us to start the Y scan immediately after X stops. That reduces build time and prevents overheating.
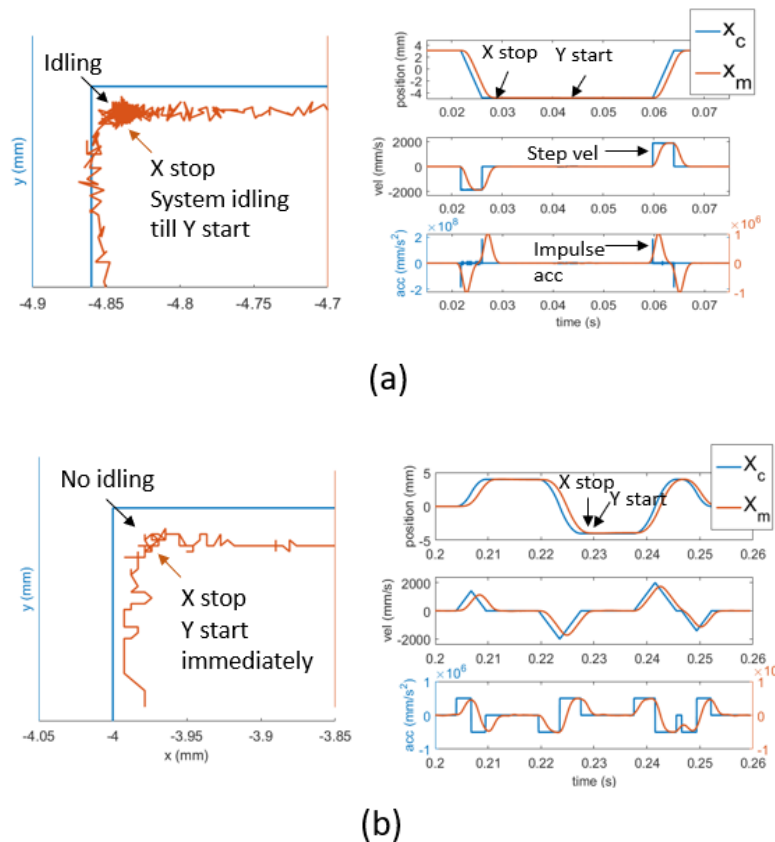

Figure 12: Commanded and measured scan position, velocity, and acceleration for (a) commercial AM controller, and (b) SAM controller. An 8 mm square was scanned. The commanded positions are plot in blue, the measured in orange. X_c, and X_m are the commanded and measured positions, respectively.

Although it is a very important topic and directly impacts the build quality, there is very little literature that can be found on how the LPBF AM control is implemented. We could only conduct very limited studies based on the equipment and tools available. Nevertheless, our goal

here is to promote open platform AM process control. We already presented our control framework and the SAM software developed following this framework. In the next section, we will use a few case studies to demonstrate its benefits.

Advanced Scan Strategy Case Studies

The AM control framework (Figure 1) and the open platform modular design (Figure 2) allow a continuous improvement of SAM software to add functions and features per research needs. In this section, we present case studies on the advanced scan strategies developed with SAM. The development of these scan strategies, however, is inspired by many excellent AM research works.

Spiral Scan Strategy

Spiral scan strategy is developed to research the effect of an unconventional, non-linear scan strategy on meltpool area and the resulting microstructure. The design of the continuous circular spiral scan path can be seen in Figure 13a. It starkly contrasts the conventional raster scan path in Figure 13b. This unconventional scan strategy is made possible through the G22 implementation in SAM. 17-4 stainless steel rectangular parts of 10 mm in length, 5 mm in width, and 10 mm in height were built with both raster and spiral scan strategies. The parts built with the spiral scan strategy show a maximum of 54% increase in hardness and a distinct microstructure. It is speculated the much larger meltpool observed and the reheating effect by the spiral scan strategy significantly changed the solidification process. The spiral scan provides a possible means to control the microstructure of the additive manufactured material. More detail of this work can be found in [17].
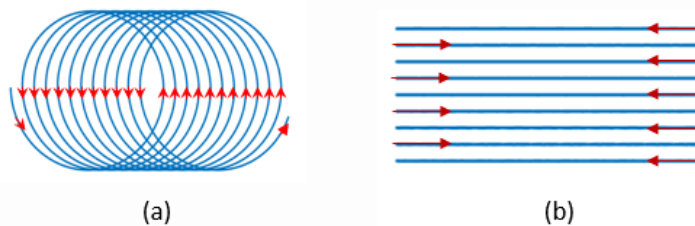

Figure 13: (a) Spiral scan strategy. (b) raster scan strategy. The arrows indicate the scan directions. The hatch space (space between the circles or the lines) is 100 µm.

Three-Dimensional Scan Strategies

Twelve nickel alloy 625 rectangular parts of 10 mm in length, 10 mm in width, and 5 mm in height were built. The goal of this work was to compare the effect of scan strategy on part quality. A different scan strategy is used for each part (Table 1). These scan strategies were composed with the SAM using the combination of its standard options in the G-code generator and G-code interpreter modules. For example, part 8 used a combination of island strategy, exact stop path mode, and constant density power mode. The process was monitored in situ by a high-speed camera coaxially aligned with the heating laser beam (Figure 6c). The galvo encoder position

was captured. All the parts were successfully built, and the time-stepped digital command and monitoring data were published [18] and used by many scan strategy studies. The parts were also measured with X-ray Computed Tomography (XCT) for porosity, and correlations between the pores and the meltpool images were attempted.

Table 1. The twelve three-dimensional scan strategies studied

1. basic, constant speed, constant power	4. Island stripe, continuous, constant power	7. Island stripe, exact stop, constant power	10. Island, alternative stripe / concentric layer, continuous, constant density
2. Island stripe, constant speed, constant power	5. Island stripe, continuous, constant density	8. Island stripe, exact stop, constant density	11. Island stripe, continuous, interleaved power, constant density
3. Island concentric, continuous, constant power	6. Island concentric, continuous, constant density	9. Island concentric, alternative power continuous, constant density	12. Island concentric, interleaved power continuous, constant density

Figure 14 compares the meltpool from parts 7 and 8, that used constant power and constant power density scan strategies, respectively. For each scan strategy, four sample meltpool images are shown on the right, while the speed, power, and meltpool image area are plotted on the left. The meltpool image area is measured by thresholding the 8-bit grayscale meltpool image at intensity level of 100. The constant power density was implemented with Equation 1, where L_o is the nominal laser power in W, L is the applied laser power in W, V is the instantaneous speed in mm/s, V_o is the nominal speed in mm/s, and C is a unitless weighting factor between 0 and 1. $C = 0.5$ is used to maintain a minimum laser power level by varying only a portion of the power to the speed since power should not drop below a threshold where the powder will not melt at any speed. It can be clearly seen from Figure 14 that the constant power density scan strategy kept the meltpool more constant when the speed slows down.

$$L = (V/V_n) \cdot C \cdot L_o + (1-C) \cdot L \tag{1}$$

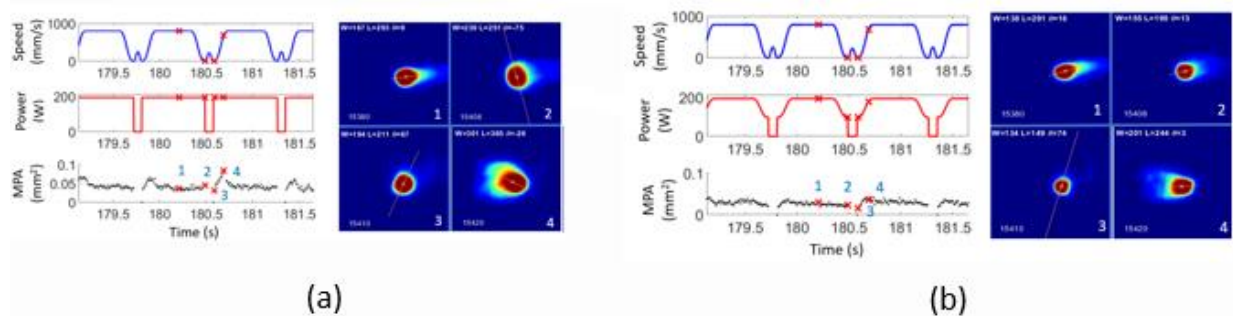(a)   (b)

Figure 14: Meltpool area plotted together with laser speed and power shown on the left, and meltpool images at locations marked by an 'x' shown on the right. (a) Constant laser power. (b) Constant power density

The constant power density scan strategy requires continuous laser power variation (intra-vector laser power control), which is made possible by the SAM G-code interpreter. The XCT results show the porosity decreased from 0.39% for the part built by constant power to 0.11% for the part built by constant power density strategy. It is believed the constant power density strategy reduces the concentration of laser energy at the end of the scan and hence prevents the formation of keyhole pores.

Geometric Conductivity Factor

When a part is built using LPBF, there are areas that have powder, melted metal, and solid metal. These areas have different thermal conductivities depending on the state of the metal and the part geometry. This can be explained by Figure 15, where voxels 1 – 4 have different conductivity, depending on whether their neighborhood is 'more' solid or powder when it is being built. A Geometric Conductivity Factor (GCF) is developed to quantify this effect. The GCF model is created solely based on the time-stepped digital command. The computer algorithm follows the command to reconstruct a 3D structure by 'melt' voxels as in Figure 15, and assigns each melt voxel a GCF value as the voxel is created (melted).
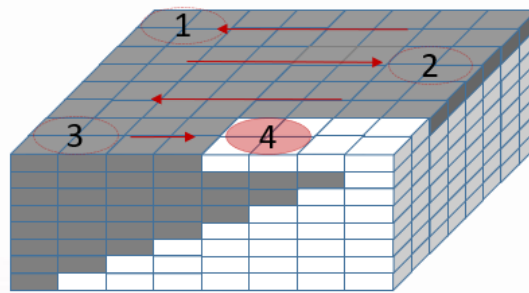

Figure 15: 3D structure reconstructed through digital command. The darker voxels are where the laser power is programmed to be on.

Using a Geometric Conductivity Factor (GCF) scan strategy, the different conductivities due to the geometric shape and build sequence can be considered. The laser power can be altered to account for these differences. Figure 16 shows an example, where a GCF model is created from the digital command of overhanging structure. The GCF values near the boundaries and the overhang regions are smaller since these regions are surrounded by powder (Figure 16a). The powder has a much lower conductivity than solidified metal [19]. The GCF is then used to adjust the laser power, as shown in Figure 16b. This is a typical example of model-based thermal adjusted power mode in SAM. The part built with the GCF scan strategy demonstrated a significant reduction in surface roughness in the overhang regions. More details on the GCF model construction and its effect on part qualities can be found in [20].
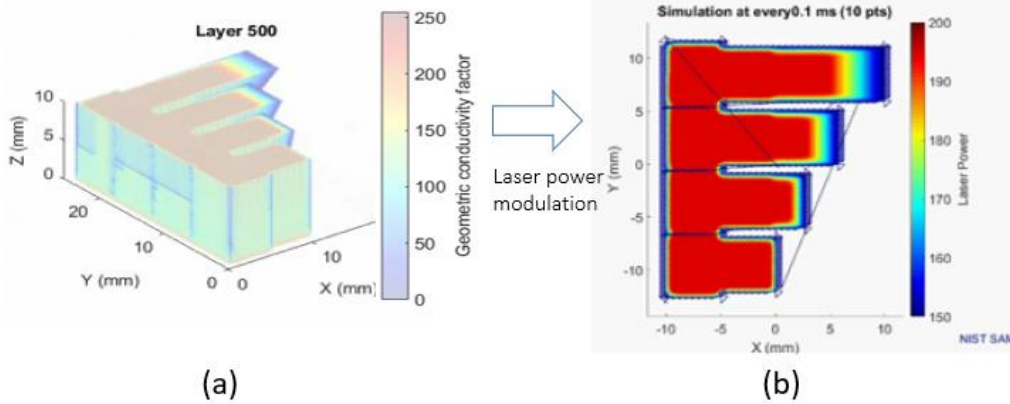
Figure 16: GCF scan strategy construction. (a) GCF model. (b) GCF optimized scan strategy for one of the layers. Laser power is represented by the pseudo color.

Residual Heat Factor

The residual heat factor (RHF) is created to account for the dynamic reheating effect. This is an effect that occurs because previous scan lines will have residual heat, affecting the thermal condition of the current scan position. The dynamic reheating effect often results in inconsistent meltpool morphology. To counteract this, a value called RHF is assigned each scan position (points in the time-stepped digital command) to 'quantify' the residual heat effect, and the laser power is adjusted based on the RHF value to reduce local variability of meltpool area. This is another example of model-based thermal adjusted power mode. The RHF concept is based on the proximity analysis feature of SAM [21], which determines the neighborhood scan points in a predefined temporal and spatial window as shown in Figure 17. The temporal window defined by the elapsed time T and spatial window defined by a radius R are drawn in the figure on the scan path. Each dot on the path is a position in the time stepped digital command. The RHF for the scan point i can be formulated as Equation 2, where d_{ki} = distance of point i from point k, t_{ki} = time elapsed between point i and point k, L_k = laser power level at point k, v_k is the velocity at point k, and S is the set of points scanned within time T and within distance R from point i.

$$\text{RHF}_i = \sum_{k \in S} \left(\frac{R - d_{ki}}{R}\right)^2 \left(\frac{T - t_{ki}}{T}\right) \frac{L_k}{v_k} \tag{2}$$
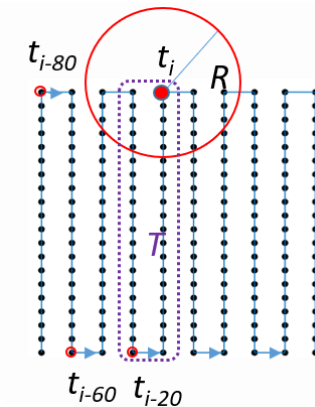

Figure 17: RHF model construction. Each dot on the scan path is a point in the time-stepped digital command. Elapsed time $< T$ is indicated by a purple dotted line and distance $< R$ indicated by a red circle, where $T = 40$ time-steps and $R = 250$ μm in this example.

RHF in Equation 2 assumed the residual heat effect from a previous point k to the current scan point is inversely proportional to the elapsed time and square of the distance. A different heat dissipation model can be used. The RHF is then normalized and used to scale the laser power. The RHF is optimized by the value of T and R, which can be done by simulation, machine learning, or experimentally. An experimental approach to RHF optimization can be found in [22]. Figure 18 shows an example, where a 3 mm x 2 mm rectangular pad was scanned without and with the RHF optimization, and the meltpool area maps are plotted in Figure 18a and Figure 18b, respectively. The variability of meltpool area is reduced by 27% (measured by the standard deviation of the meltpool area) by the RHF optimization, and this reduction can be clearly seen by comparing Figure 18a and Figure 18b.
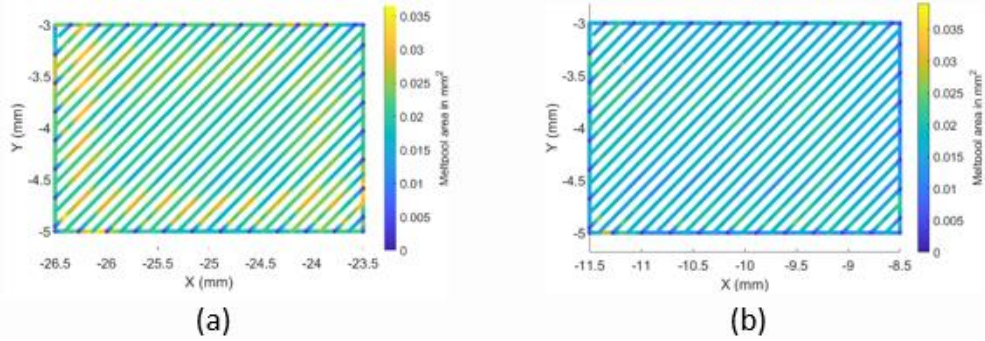

Figure 18: Meltpool area map for a rectangular pad scan. The meltpool area is represented by pseudo color. (a) Without RHF optimization. (b) With RHF optimization.

Machine Learning

The RHF concept can also be used to formulate a data-driven meltpool area predictive function, such as Equation 3, where S_i is the meltpool size for scan point i in the time-stepped digital command, and L_i is the laser power, v_i is the scan speed, $\theta_i^{\Delta d}$ and $\theta_i^{\Delta t}$ represent the cumulative residual heat effect based on spatial difference Δd and time difference Δt. They can be represented as $\theta_i^{\Delta d} = \sum_{k \in S}(\frac{R-d_{ki}}{R})^2 \frac{L_k}{v_k}$ and $\theta_i^{\Delta t} = \sum_{k \in S}(\frac{T-t_{ki}}{T})\frac{L_k}{v_k}$ as in the RHF definition (Equation 2). A different representation can also be used, such as in our meltpool prediction based scan strategy study [23], in which $\theta_i^{\Delta d}$ is dropped to prevent overfitting, and $\theta_i^{\Delta t}$ is put as $\sum_{k \in S}(e^{a_t t_{ki}})\frac{L_k}{v_k}$, where a_t is a constant which can be determined from the experiment.

$$S_i = f(L_i, v_i, \theta_i^{\Delta t}, \theta_i^{\Delta d}) \tag{3}$$

Once a meltpool area prediction model is trained, it can be used to adjust the laser power in the time-stepped digital command until the calculated meltpool area is within the objective, or the power constraint reached. A combination of objective meltpool area and constraint of power was tested in [23]. The results are shown in Table 2 together with the original scan strategy. The original scan strategy used in this exercise is the island concentric, continuous, and constant power density strategy from #6 in Table 1. Scenario #6 in Table 2 gives the most consistent meltpool area, a 78% improvement in the meltpool area standard deviation (SD) when compared to the original.

Table 2. Experimental results for original and optimized scan strategy

Scenario	Constraint of power (W)	Objective meltpool area (mm^2)	Measured meltpool area Mean $\pm$ SD (mm^2)
Original	N/A	N/A	0.0304 ± 0.0181
1	100-195	$0.014 - 0.026$	0.0231 ± 0.0075
2	100-195	$0.016 - 0.024$	0.0221 ± 0.0073
3	100-195	$0.018 - 0.022$	0.0208 ± 0.0069
4	50-250	$0.014 - 0.026$	0.0208 ± 0.0044
5	50-250	$0.016 - 0.024$	0.0203 ± 0.0044
6	50-250	$0.018 - 0.022$	0.0193 ± 0.0039

There are more recent studies by others on scan strategy optimization by compensating residual heat using the machine learning approach [24,25]. These are excellent works, but there is a lack of experimental verification. Most commercial systems do not accept user-optimized scan strategies. This is also true for testbeds developed with commercial galvo controllers; user customization can only stay at the scan line level since there is no access to in-line control. The NIST AM framework (Figure 2) uses time-stepped digital commands as process control files, which supports user customization down to each scan point. The pointwise control in the time-stepped digital command (Figure 4) by its nature supports the machine learning-based optimization method very well.

Conclusion and Future Work

An additive manufacturing (AM) control software, Simple AM (SAM), is developed. SAM consists of four modules: slicing, planning, interpolation, and simulation. The slicing module slices the STL file and outputs a vertices file that contains the vertices of all the layers sliced. An AM G-code standard is proposed, adding the laser power and laser spot diameter control on top of the position and speed control of conventional G-code. The planning module generated scan path and power to cover the regions described by the vertices file and output the results as AM G-code. A time-stepped digital command file format is also defined, consisting of galvo X-Y position, laser power, laser diameter, and periphery device trigger updates in 10 µs incremental time steps. An AM G-code interpreter is developed to convert AM G-code to time-stepped digital command based on different velocity profiles, path modes, and power modes. This is also known as interpolation. The time-stepped digital command file can be sent directly to execute on the AM machine, or verified on the simulation module.

Laser powder bed fusion additive manufacturing is a very delicate process. A small deviation from the optimum condition could trigger defects and deteriorate the part quality. Such deviation can be caused by inadequate process control, such as a power concentration at the end of the scan, or a change in the thermal properties, such as a change of conductivity over an overhang region. We demonstrated how these situations are handled through different case studies. One common requirement in these studies is the in-line power control, which is made possible by the SAM interpreter and the time-stepped digital command. The time-stepped digital command allows a point-wise control of the AM process, versus the line-wise control which is commonly

used on AM machines today. Moreover, the time-stepped digital command also facilitates model-based scan strategy optimization.

One uniqueness of our work is the jerk-limited motion control; it improves both spatial and temporal position accuracies, hence enabling an accurate laser power-position synchronization. This established the foundation of advanced AM control. The motion control on commercial systems was compared. It is found that the step velocity profile was used for the motion control on all three systems we evaluated. It is interesting to see how the overshoot path and idling time are used to prevent the following errors and improve spatial accuracy. These limit the flexibilities in scan strategy but allows a very computationally efficient path interpolation. Nevertheless, computational efficiency may no longer be an issue on a modern numerical controller with improved computational performance. The same is true for the data storage; the large file size of the time-stepped digital command is less and less of a concern.

There are many opportunities to improve the field of laser powder bed fusion (LPBF) additive manufacturing. More research into the laser scan strategies has the potential to develop repeatable ways to produce high-quality parts with minimal defects, controlled residual stress or microstructure, and improved speed and efficiency of material consolidation. The open platform software gives researchers the maximum flexibility possible and maximum control over process parameters. Many built-in features of SAM have not been tested/optimized. The machine learning scan strategy optimization also seems very promising. These are the directions we are continuously working toward.

Reference

[1] Badiru AB, Valencia VV, Liu D, editors. Additive Manufacturing Handbook: Product Development for the Defense Industry. 1st ed. CRC Press; 2017. https://doi.org/10.1201/9781315119106.
[2] Oliveira JP, LaLonde AD, Ma J. Processing parameters in laser powder bed fusion metal additive manufacturing. Materials & Design 2020;193:108762. https://doi.org/10.1016/j.matdes.2020.108762.
[3] King WE, Barth HD, Castillo VM, Gallegos GF, Gibbs JW, Hahn DE, et al. Observation of keyhole-mode laser melting in laser powder-bed fusion additive manufacturing. Journal of Materials Processing Technology 2014;214:2915–25.
[4] Gong H, Rafi K, Gu H, Starr T, Stucker B. Analysis of defect generation in Ti–6Al–4V parts made using powder bed fusion additive manufacturing processes. Additive Manufacturing 2014;1–4:87–98. https://doi.org/10.1016/j.addma.2014.08.002.
[5] Thijs L, Verhaeghe F, Craeghs T, Humbeeck JV, Kruth J-P. A study of the microstructural evolution during selective laser melting of Ti–6Al–4V. Acta Materialia 2010;58:3303–12. https://doi.org/10.1016/j.actamat.2010.02.004.
[6] Yadroitsev I, Thivillon L, Bertrand P, Smurov I. Strategy of manufacturing components with designed internal structure by selective laser melting of metallic powder. Applied Surface Science 2007;254:980–3. https://doi.org/10.1016/j.apsusc.2007.08.046.
[7] Li C, Liu ZY, Fang XY, Guo YB. Residual Stress in Metal Additive Manufacturing. Procedia CIRP 2018;71:348–53. https://doi.org/10.1016/j.procir.2018.05.039.
[8] Cheng B, Shrestha S, Chou K. Stress and deformation evaluations of scanning strategy effect in selective laser melting. Additive Manufacturing 2016;12:240–51. https://doi.org/10.1016/j.addma.2016.05.007.

[9] Gockel J, Beuth J. Understanding Ti-6Al-4V microstructure control in additive manufacturing via process maps. Solid Freeform Fabrication Proceedings Solid Freeform Fabrication Proceedings (Austin, TX) Pp 666–74 n.d.

[10] Platt S, Wegner J, Kleszczynski S, Witt G. Effect of scan strategy, re-melting and exposure time on the microstructure of stainless steel 17 - 4 PH fabricated by laser powder bed fusion of metals. 7th International Conference on Additive Technologies ICAT 2018At: Maribor, Slovenia n.d.

[11] Lane et al. Design, Developments, and Results from the NIST Additive Manufacturing Metrology Testbed (AMMT). Solid Freeform Fabrication 2016: Proceedings of the 26th Annual International Solid Freeform Fabrication Symposium n.d.

[12] Smid P. CNC programming handbook: a comprehensive guide to practical CNC programming. 3rd ed. New York, NY: Industrial Press; 2008.

[13] Kramer TR, Proctor FM, Messina ER. The NIST RS274NGC Interpreter – Version 3 n.d.

[14] EIA Standard RS-274-D. Interchangeable Variable Block Data Format for Positioning, Contouring, and Contouring/Positioning Numerically Controlled Machines 1979.

[15] Yeung H, Lane BM, Donmez MA, Fox JC, Neira J. Implementation of Advanced Laser Control Strategies for Powder Bed Fusion Systems. Procedia Manufacturing 2018;26:871–9. https://doi.org/10.1016/j.promfg.2018.07.112.

[16] Yeung H, Lane B, Fox J, Kim F, Heigel J, Neira J. Continuous laser scan strategy for faster build speeds In laser powder bed fusion system. Solid Freeform Fabrication 2017: Proceedings of the 28th Annual International Solid Freeform Fabrication Symposium n.d.

[17] Yeung H, Chen J, Yang G, Guo Y, Lin D, Tan W, et al. Effect of spiral scan strategy on microstructure for additively manufactured stainless steel 17–4. Manufacturing Letters 2021;29:1–4. https://doi.org/10.1016/j.mfglet.2021.04.005.

[18] Lane B, Yeung H. Process Monitoring Dataset from the Additive Manufacturing Metrology Testbed (AMMT): "Three-Dimensional Scan Strategies." J RES NATL INST STAN 2019;124:124033. https://doi.org/10.6028/jres.124.033.

[19] Zhang S, Lane B, Whiting J, Chou K. On thermal properties of metallic powder in laser powder bed fusion additive manufacturing. Journal of Manufacturing Processes 2019;47:382–92. https://doi.org/10.1016/j.jmapro.2019.09.012.

[20] Yeung H, Lane B, Fox J. Part geometry and conduction-based laser power control for powder bed fusion additive manufacturing. Additive Manufacturing 2019;30:100844. https://doi.org/10.1016/j.addma.2019.100844.

[21] Yeung H, Neira J, Lane B, Fox J, Lopes F. Laser Path Planning And Power Control Strategies For Powder Bed Fusion Systems. Proceedings of the 27th Annual International Solid Freeform Fabrication Symposium n.d.

[22] Yeung H, Lane B. A residual heat compensation based scan strategy for powder bed fusion additive manufacturing. Manufacturing Letters 2020;25:56–9. https://doi.org/10.1016/j.mfglet.2020.07.005.

[23] Yeung H, Yang Z, Yan L. A Meltpool Prediction Based Scan Strategy for Powder Bed Fusion Additive Manufacturing. Additive Manufacturing 2020:101383. https://doi.org/10.1016/j.addma.2020.101383.

[24] Demir K, Zhang Z, Ben-Artzy A, Hosemann P, Gu GX. Laser scan strategy descriptor for defect prognosis in metal additive manufacturing using neural networks. Journal of Manufacturing Processes 2021;67:628–34. https://doi.org/10.1016/j.jmapro.2021.05.011.

[25] Stathatos E, Vosniakos G-C. Real-time simulation for long paths in laser-based additive manufacturing: a machine learning approach. Int J Adv Manuf Technol 2019;104:1967–84. https://doi.org/10.1007/s00170-019-04004-6.